Multiple transpolar auroral arcs reveal insight about coupling processes in the Earth's magnetotail

Qing-He Zhang[a,1], Yong-Liang Zhang[b], Chi Wang[c], Michael Lockwood[d], Hui-Gen Yang[e], Bin-Bin Tang[c], Zan-Yang Xing[a], Kjellmar Oksavik[f,g], Larry R. Lyons[h], Yu-Zhang Ma[a], Qiu-Gang Zong[i], Jøran Idar Moen[j,g], and Li-Dong Xia[a]

[a]Shandong Provincial Key Laboratory of Optical Astronomy and Solar-Terrestrial Environment, Institute of Space Sciences, Shandong University, Weihai, Shandong, 264209, China; [b]The Johns Hopkins University Applied Physics Laboratory, Laurel, MD 20723; [c]State Key Laboratory of Space Weather, Center for Space Science and Applied Research, Chinese Academy of Sciences, Beijing, 100190, China; [d]Department of Meteorology, University of Reading, Reading, RG6 6BB, United Kingdom; [e]Ministry of Natural Resources Key Laboratory of Polar Science, Polar Research Institute of China, Shanghai, 200136, China; [f]Department of Physics and Technology, Birkeland Centre for Space Science, University of Bergen, Bergen, N-5020, Norway; [g]Arctic Geophysics Department, The University Centre in Svalbard, Longyearbyen, N-9171, Norway; [h]Department of Atmospheric and Oceanic Sciences, University of California, Los Angeles, CA 90095; [i]School of Earth and Space Sciences, Peking University, Beijing, 100871, China; and [j]Department of Physics, University of Oslo, Blindern, Oslo 0371, Norway

Edited by Lennard A. Fisk, University of Michigan, Ann Arbor, MI, and approved May 26, 2020 (received for review January 11, 2020)

A distinct class of aurora, called transpolar auroral arc (TPA) (in some cases called "theta" aurora), appears in the extremely high-latitude ionosphere of the Earth when interplanetary magnetic field (IMF) is northward. The formation and evolution of TPA offers clues about processes transferring energy and momentum from the solar wind to the magnetosphere and ionosphere during a northward IMF. However, their formation mechanisms remain poorly understood and controversial. We report a mechanism identified from multiple-instrument observations of unusually bright, multiple TPAs and simulations from a high-resolution three-dimensional (3D) global MagnetoHydroDynamics (MHD) model. The observations and simulations show an excellent agreement and reveal that these multiple TPAs are generated by precipitating energetic magnetospheric electrons within field-aligned current (FAC) sheets. These FAC sheets are generated by multiple-flow shear sheets in both the magnetospheric boundary produced by Kelvin–Helmholtz instability between supersonic solar wind flow and magnetosphere plasma, and the plasma sheet generated by the interactions between the enhanced earthward plasma flows from the distant tail (less than −100 R_E) and the enhanced tailward flows from the near tail (about −20 R_E). The study offers insight into the complex solar wind-magnetosphere-ionosphere coupling processes under a northward IMF condition, and it challenges existing paradigms of the dynamics of the Earth's magnetosphere.

aurora | solar–terrestrial interaction | magnetosphere | polar ionosphere | transpolar auroral arcs

Transpolar arcs (TPAs) are the large-scale auroral forms that stretch almost entirely across the polar cap and connect the dayside and nightside auroral oval (1–5). TPAs can appear as a single or multiple arcs (6–8). Previous theories and observations indicated that TPAs are related to the magnetospheric cusp as their dayside ends join together in the cusp region (called "cusp-aligned" auroral arcs) (9, 10), and are generated by the solar wind–magnetosphere–ionosphere coupling processes as a whole system during northward interplanetary magnetic field (IMF) and quiet geomagnetic conditions (2–5). TPAs are sometimes seen simultaneously in both polar caps (11) and have been inferred to be on both open and closed magnetic field lines (12).

TPA formation processes have long been debated, in particular whether they are driven by dayside or nightside processes (5). The main candidates for dayside processes have been dayside reconnection at the low-latitude magnetopause or high-latitude lobe regions (13–17) and plasma instabilities (e.g., Kelvin–Helmholtz instability, interchange instability) near the magnetospheric low and high-latitude boundary layers (8, 18–20). The main candidates for nightside processes have been proposed as nightside reconnection in the magnetotail (4, 7) and twisting of the magnetotail due to IMF variations (3, 21, 22). These processes could result in plasma sheet bifurcation, filamentary extent into the lobes, or hot plasma trapped in the tail lobes (1, 7, 23–25). None of the suggested processes can explain all of the observed characteristics, and especially multiple TPAs. It has also been difficult to investigate the phenomenon due to constraints on obtaining simultaneous observations at multiple points across the solar wind–magnetosphere–ionosphere system. Here, we present ground-breaking multiple-instrument observations of multiple TPAs structures seen simultaneously both in the ionosphere and the distant magnetotail. The observations are interpreted using a global three-dimensional (3D) magnetohydrodynamic (MHD) simulation, giving for a discussion of the formation of multiple TPAs from a global perspective.

On 7 September 2017, long-lasting, relatively stable northward IMF conditions (IMF $B_z > 0$ for more than 8 h) occurred with comparable dawn–dusk components (IMF B_y) and roughly stable solar wind conditions, except for some IMF variations and

Significance

Colorful and dynamic aurora has attracted human's attention since the dawn of time. However, mystery remains in understanding a distinct class of aurora, transpolar auroral arc (TPA) (or "theta" aurora) which occurs in extremely high latitude of the Earth polar regions when interplanetary magnetic field (IMF) is northward. Previous theories are unable to explain why multiple TPAs often occur. Our comprehensive observations in the ionosphere and magnetotail as well as a three-dimensional magnetosphere modeling shed insight on how multiple TPAs form. Our study offers clues how solar wind energy and mass transfer into the magnetosphere and ionosphere under a northward IMF that occurs nearly half of the time.

Author contributions: Q.-H.Z. and Y.-L.Z. designed and performed research; C.W. and B.-B.T. contributed new reagents/analytic tools; Q.-H.Z., Y.-L.Z., H.-G.Y., Z.-Y.X., K.O., and Y.-Z.M. analyzed data; Q.-H.Z., Y.-L.Z., C.W., M.L., H.-G.Y., B.-B.T., Z.-Y.X., K.O., L.R.L., Y.-Z.M., Q.-G.Z., J.I.M., and L.-D.X. participated in the scientific discussions; and Q.-H.Z., Y.-L.Z., M.L., K.O., and L.R.L. wrote the paper.

The authors declare no competing interest.

This article is a PNAS Direct Submission.

Data deposition: The 3D MHD simulation data are available on the website of https://zenodo.org/record/3777265# with a separate DOI of 10.5281/zenodo.3777265. The time sequence of 557.7-nm aurora images from the all-sky imager at the Chinese Antarctic Zhongshan Station (ZHS) are available on the website of https://zenodo.org/record/3778095# with a separate DOI of 10.5281/zenodo.3778095.

[1]To whom correspondence may be addressed. Email: zhangqinghe@sdu.edu.cn.

This article contains supporting information online at https://www.pnas.org/lookup/suppl/doi:10.1073/pnas.2000614117/-/DCSupplemental.

dynamic pressure increases around 12:30 UT (Fig. 1 *A*–*C*). The northward IMF reached around 8 nT and was roughly stable, with the B_y component around 4 nT, and a high solar wind speed of around 520 km/s (see gray shading in Fig. 1 indicating the interval of interest). These conditions are favorable for triggering of the Kelvin–Helmholtz instability between the solar wind and magnetosphere (26–29) and multiple cusp-aligned auroral arcs in the polar cap (9, 10). The auroral electrojet AL and AU indices, the smallest (AL) and largest (AU) values of geomagnetic variations in the horizontal component observed at 11 selected observatories along the auroral zone in the northern hemisphere, show nonsubstorm conditions after 15:30 UT (Fig. 1*D*), indicating a quiet auroral oval.

Auroral observations from the Southern Hemisphere are presented in Fig. 2 *A*–*E*. Poleward of a normal auroral oval at lower latitudes, Fig. 2*A* shows at least six bright TPAs in the otherwise empty polar cap (poleward of −78° MLAT, and highlighted by gray shading in Fig. 2 *F*–*H*) from Defense Meteorological Satellite Program (DMSP) F17 Special Sensor UV Spectrographic Imager (SSUSI) data. In addition, there are several radially aligned arcs both within the dawnside (−70 to −78° MLAT) and duskside (−70 to −77° MLAT) auroral oval. Several of the TPAs were brighter than the main auroral oval with brighter spots within them and persisted for more than 2 h including their evolution and decay (*SI Appendix*, Fig. S1 *B*–*D*). Fig. 2 *B*–*E* shows the time evolution of the aurora during an overflight by the DMSP F17 spacecraft of one TPA, as recorded by a 557.7-nm all-sky imager at the Chinese Antarctic Zhongshan Station (ZHS) (30). The projected field-aligned current (FAC) along the satellite track suggests that each arc was associated with an upward FAC (Fig. 2 *A* and *F*). Minor offsets can be attributed to altitude differences between the two datasets. The in situ plasma observations of the electron energy flux (Fig. 2*G*) show that each auroral arc was associated with precipitation of electrons that have been accelerated to more than 1 keV. Most of the TPAs were not associated with observable ion precipitation, but may be associated with upward ion beams observed by Cluster satellites in other events (31, 32). The electron energy fluxes (Fig. 2*G*) also reveal several smaller arcs that were not visible in the DMSP/SSUSI images with a limited spatial resolution and/or sensitivity (Fig. 2*A*). The formation of such multiple/filamentary TPAs has remained an intriguing and unresolved puzzle for many years.

Using the measured interplanetary conditions as input, a high-resolution 3D global MHD code called Piecewise Parabolic Method with a Lagrangian Remap to MHD (PPMLR-MHD) (33, 34), was run to investigate the formation of multiple TPAs. An electrostatic ionosphere shell with height-integrated conductance is imbedded in the MHD code, allowing for the electrostatic coupling and calculation of FACs between the ionosphere, which is near the Earth, and the model's magnetospheric inner boundary. Fig. 3*A* shows a two-dimensional extract from a movie (Movie S1) of simulated FACs and plasma velocity vectors in the Geocentric Solar Magnetosphere (GSM) X-Y plane [$Z \sim -1$ R_E for better capturing the phenomenon in the Southern Hemisphere (35)]. The magnetotail is to the left, and the subsolar magnetopause is to the right. Pairs of strong and filamentary FACs are shown in red and blue color, generated by flow shear sheets around the dayside magnetopause at both flanks in the low-latitude boundary layer (LLBL) due to the Kelvin-Helmholtz instability (KHI), and newly formed flow shear and FAC sheets are added while the previous shear sheets are gradually pushed inward and tailward resulting in multiple FACs sheets in the LLBL (Movie S1). Some of these FACs merge with the existing FACs; others remain distinct and fade. These upward FACs cause magnetic field-aligned acceleration of magnetospheric electrons [probably through the Knight's current-voltage process (36, 37)] that precipitate into the polar ionosphere and generate the poleward-moving aurora arcs in the

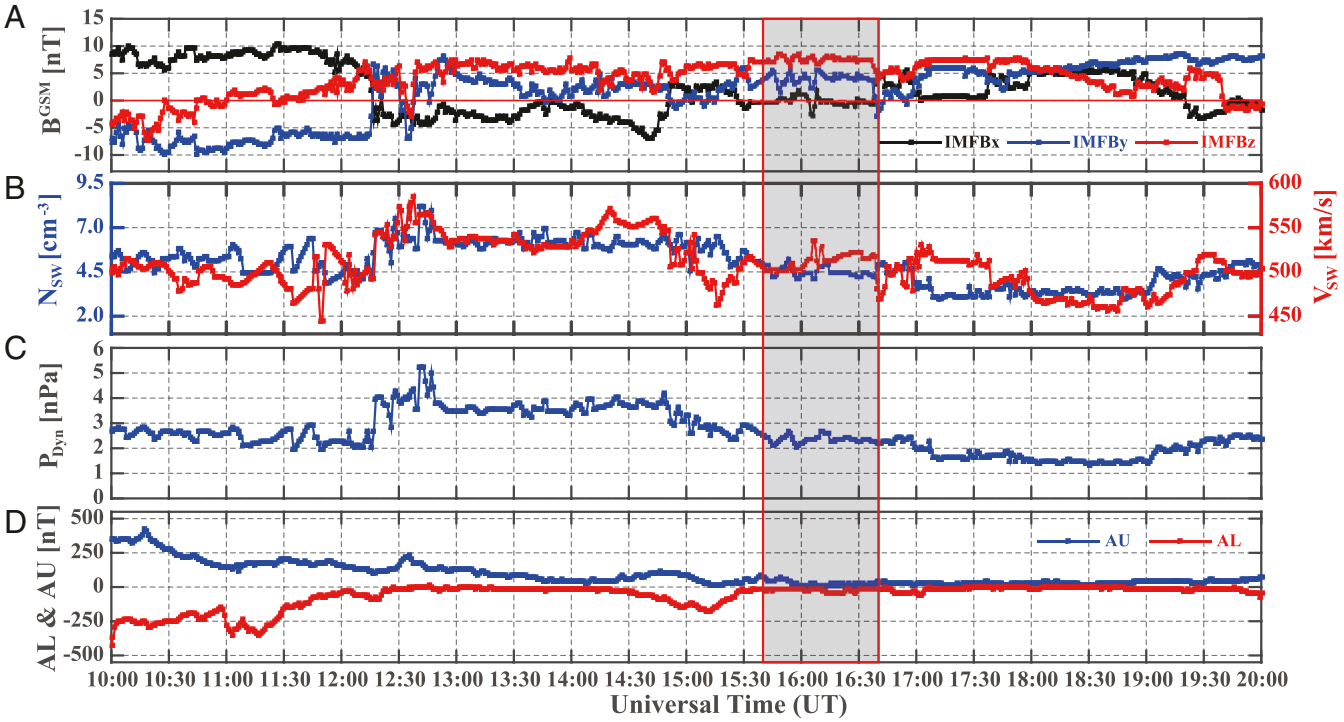

Fig. 1. An overview of the interplanetary conditions and auroral electrojet indices on 7 September 2017 from NASA OMNIWeb. (*A*) The IMF components in GSM coordinates; (*B*) the solar wind number density and speed; (*C*) the solar wind dynamic pressure, P_{Dyn}; and (*D*) the provisional auroral electrojet geomagnetic indices (from 11 stations): red and blue lines are for AU and AL. Interplanetary data have been lagged by 5 min to allow for propagation from the nose of the bow shock to the dayside magnetopause.

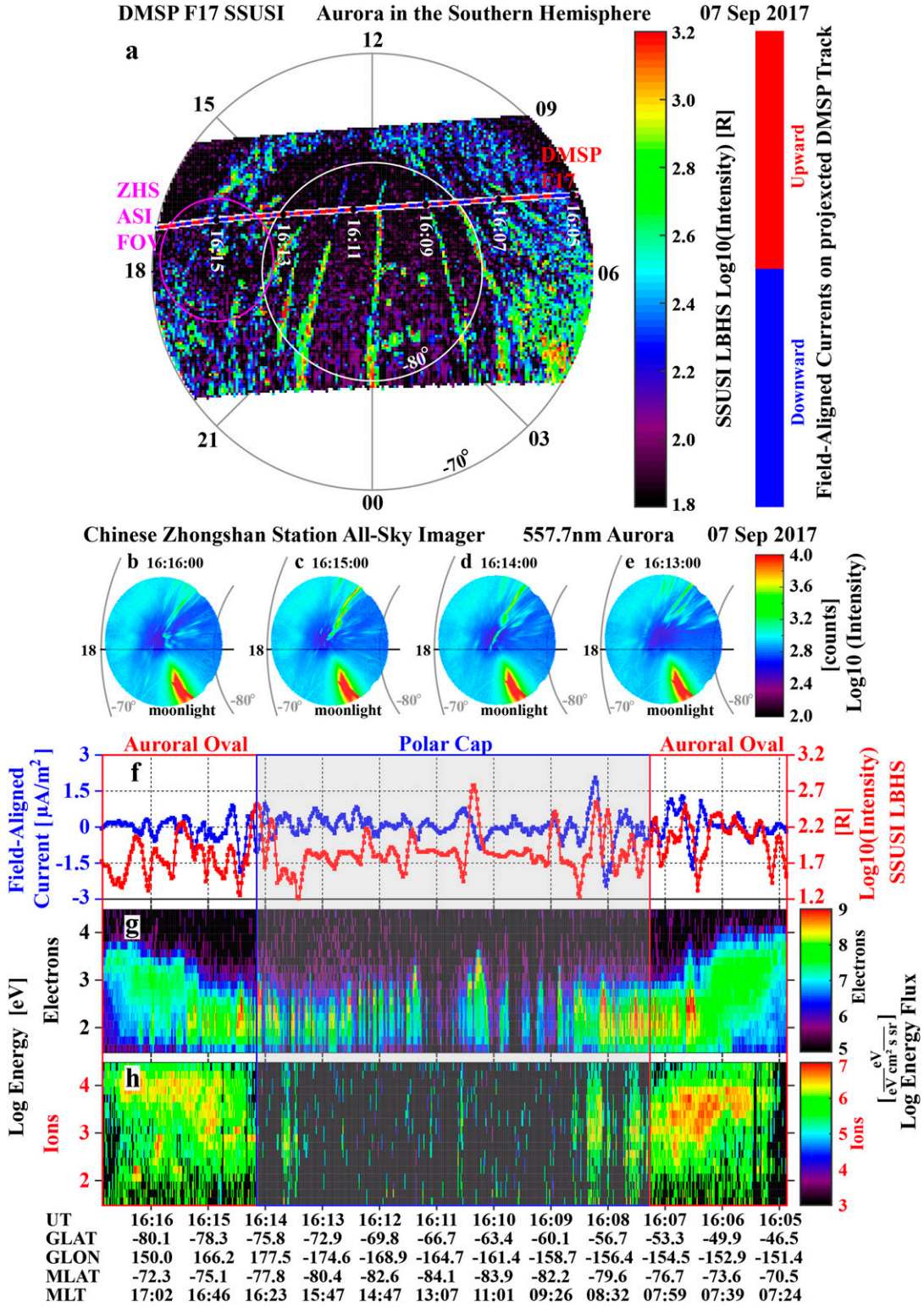

Fig. 2. Aurora and in situ plasma and FAC observations in the Southern Hemisphere. (*A*) Aurora in the Lyman–Birge–Hopfield short-band (LBHS) band (wavelength of 140–150 nm) observed by the SSUSI instrument on board the DMSP F17 satellite from JHU/APL and the sign of the FACs shown in red and blue color along the satellite track. The FAC is calculated from the special sensor microwave (SSM) magnetic field measurement on board the satellite, (*B–E*) sequence of 557.7-nm aurora images from the all-sky imager at the ZHS, (*F*) time series of the calculated FACs and the aurora intensity extracted from A along the track of DMSP F17, and (*G*) and (*H*) electron and ion energy flux spectrograms from JHU/APL special sensor for precipitating particles (SSJ5) instrument on board the DMSP F17. The magenta ellipse in *A* shows the field of view (FOV) of the ZHS all-sky imager. *B–H* are shown in the reversed order to better align with the DMSP F17 trajectory in *A*; i.e., time runs from the right to the left (dusk to the left, dawn to the right).

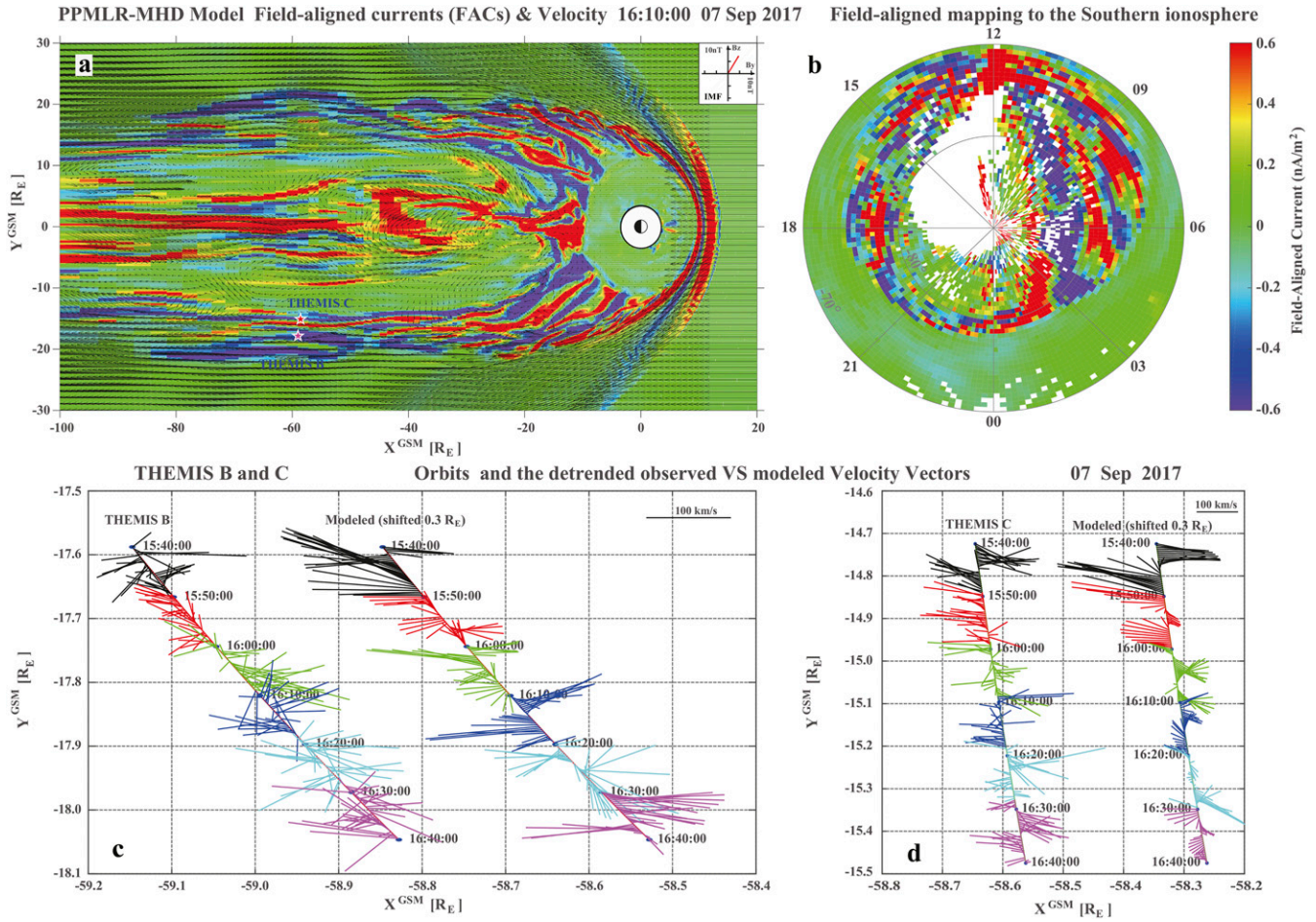

Fig. 3. An extract from a movie of the simulated FACs and plasma velocity vectors in the X-Y plane in GSM coordinates. (*A*) The 2D distribution of FACs and plasma velocity vectors in the equatorial plane of the magnetosphere simulated by the PPMLR-MHD code; (*B*) field-aligned mapping of the FACs from the equatorial plane of the magnetosphere to the ionosphere in the Southern Hemisphere; (*C*) and (*D*) the time series of the detrended plasma velocity vectors observed by the THEMIS *B* and *C* satellites and PPMLR-MHD model simulation results near the satellites locations (marked by red stars in *A*). The vectors in *C* and *D* are shown using different colors every 10 min. Both the observations and the simulation results are shown at 20-s time resolution, and the simulation results have been offset by 0.3 R_E in the X direction in *C* and *D* for easier comparison.

auroral oval (seen in Fig. 2 *A*–*E*). Meanwhile, a narrow and roughly stable upward FAC appears around Y = 0 R_E and extends down the magnetotail from X = −10 to −100 R_E at the beginning, which starts to locally break up inside the center plasma sheet at about −20 R_E in association with enhanced tailward flows from about 15:10 UT. Then at about 15:45 UT, strong bursts of earthward flow come in from the distant tail (less than −100 R_E, Movie S1). When these earthward and tailward flows with FACs encounter each other around −35 R_E, they split and form multiple flow shear and FAC sheets that extend along the dawn and dusk flanks of the magnetotail and merge with those developed by the flank KHI (Movie S1), which lead to a complex current system dominated by FACs (*SI Appendix*, Fig. S2 and Movie S1). These result in a large number of filamentary FACs and associated flow shears that populate the magnetotail (including the plasma sheet and lobes, Fig. 3*A*), making them candidate sources for the strong and structured electron precipitations that generate the multiple auroral arcs in the polar cap and auroral oval.

When the FACs are mapped along the magnetic field to the ionosphere in the Southern Hemisphere, a striking pattern emerges (Fig. 3*B* and Movie S2). The mapped FACs show clear cusp-aligned, "arclike" structures in both the polar cap and the auroral oval that are similar in shape and size to the observed arcs shown in Fig. 2*A*. A few selected points on the arclike FAC structures have been mapped back to the X-Y plane (seen in *SI Appendix*, Fig. S3). This shows that the filamentary FACs in the central magnetotail map to the central polar cap and are directly associated with the structures having the appearance of multiple TPAs. On the other hand, the filamentary FACs in the magnetospheric boundary layer map to the auroral oval and are associated with discrete arcs in the auroral oval. The white blank area in the afternoon sector polar cap of Fig. 3*B* is indicative of magnetic field lines that did not cross the X-Y equatorial plane, due to a significant IMF B_y component resulting in a distorted magnetotail and/or out of the simulation region.

To verify the simulation results we present simultaneous observations from spacecraft B and C of the THEMIS (Time History of Events and Macroscale Interactions during Substorms) mission (38) near the equatorial plane in the dawnside magnetotail. These spacecraft were in an orbit around the moon at [−59.0, −17.8, 4.0] and [−58.6, −15.1, 3.8] R_E GSM, respectively. Red stars in Fig. 3*A* mark the locations of each spacecraft, which both observed multiple flow shears in the X-Y plane that remarkably well resemble those from the KHI within the model (Fig. 3 *C* and *D*). In this analysis, the data have been detrended by subtracting the mean velocity. The results confirm

that there is indeed strong flow shears in the magnetospheric boundary layer, triggering KHI between the solar wind and magnetosphere. Both the simulation results and the THEMIS observations show very similar behavior (Fig. 3 *C* and *D*, and *SI Appendix*, Fig. S4), which adds confidence that the PPMLR-MHD model is indeed capturing the key physical processes for these northward IMF conditions.

The observations and simulation confirm the existence of strong multiple flow shears in the entire magnetosphere from the magnetopause, the lobe, and the magnetotail under a northward IMF condition. These flow shears directly lead to multiple FAC sheets that join together in the cusp region in both hemispheres and field-aligned acceleration of electrons which create multiple cusp-aligned auroral arcs both in the polar cap and auroral oval. This is a general mechanism for the formation of auroral arcs due to field-aligned acceleration of electrons through the Knight's current-voltage process (36, 37) caused by the FAC sheets that are generated by the strong flow shears in the magnetosphere (31, 32, 39–41). With a roughly stable IMF and fast solar wind speed conditions, the stable and multiple transpolar arcs, presented in this paper, cannot be fully explained by the previous models or theories, for example, the twisting magnetotail model due to IMF B_y switching (3, 21, 22), the model of tail reconnection during IMF northward nonsubstorm intervals (4, 7), and the interchange instability model (18, 19), as well as the simulation model of small-scale sun-aligned arcs on closed field lines (25). The processes, presented in this paper, operate on either open or closed field lines, indicating TPAs can occur on any field line, regardless if they are open or closed as long as there are strong plasma flow shears. This resolves the decades-long controversy: TPAs on open versus closed field lines. This study also indicates that space- and ground-based auroral observations provide a genuine way to monitor and investigate the solar wind–magnetosphere–ionosphere coupling processes, which is truly occurring across a wide range of temporal and spatial scales, under a northward IMF.

Method: PPMLR-MHD Model

The PPMLR-MHD model is based on an extension of the piecewise parabolic method (42) with a Lagrangian remap to MHD (33, 34). It is a 3D MHD model, designed specially for the solar wind–magnetosphere–ionosphere system (27–29). The model possesses a high resolution in capturing MHD shocks and discontinuities and a low numerical dissipation in examining possible instabilities inherent in the system (27).

The model uses a Cartesian coordinate system with the Earth's center at the origin and X, Y, and Z axes pointing toward the sun, the dawn–dusk direction, and the north, respectively. The size of the numerical box extends from 30 R_E to –100 R_E along the sun–Earth line and from –50 R_E to 50 R_E in Y and Z directions, with 320 × 320 × 320 grid points and a minimum grid spacing of 0.15 R_E. An inner boundary of radius 3 R_E is set for the magnetosphere to avoid the complexities associated with the plasmasphere and large MHD characteristic velocities from the strong magnetic field (29). An electrostatic ionosphere shell with height-integrated conductance is imbedded, allowing an electrostatic coupling process introduced between the ionosphere and the magnetospheric inner boundary. The Earth's magnetic field is approximated by a dipole field with a dipole moment of 8.06×10^{22} A/m in magnitude. The model is run to solve the whole system by inputting the real interplanetary conditions for the current event.

Data Availability. The solar wind and IMF data are available on the NASA OMNIWeb: https://omniweb.gsfc.nasa.gov/form/omni_min.html.

The DMSP SSUSI data are available on the Johns Hopkins University Applied Physics Laboratory website at https://ssusi.jhuapl.edu/data_retriver?spc=f17&type=edr-aur-pred&year=2017&Doy=250.

The DMSP particle data is available on the Madrigal database at http://cedar.openmadrigal.org/madExperiment.cgi/?exp=experiments3/2017/dms/06sep17&displayLevel=0&expTitle=DMSP.

The 3D MHD simulation data are available on the website of https://zenodo.org/record/3777265# with a separate DOI of 10.5281/zenodo.3777265.

The time sequence of 557.7-nm aurora images from the all-sky imager at the Chinese Antarctic ZHS are available on the website of https://zenodo.org/record/3778095#. with a separate DOI of 10.5281/zenodo.3778095.

The THEMIS satellite data are available on the website of http://themis.ssl.berkeley.edu/data/themis/thb/l2/esa/2017/.

ACKNOWLEDGMENTS. The work in China was supported by the National Natural Science Foundation (Grants 41874170, 41574138, 41604139, and 41431072), the young top-notch talent program of the "National High-level personnel of special support program (Ten Thousand Talent Program)" and the Chinese Meridian Project, and the Specialized Research Fund for State Key Laboratories of China and National Key Laboratory of Electromagnetic Environment. The work of M.L. was supported by Research Councils United Kingdom Science and Technology Facilities Council Consolidated Grant ST/M000885/1. The Norwegian contribution was supported by the Research Council of Norway Grants 223252 and 230996. The computations were performed by Numerical Forecast Modeling Research & Development and Virtual Reality System of State Key Laboratory of Space Weather. We acknowledge NASA Contract NAS5-02099 and V. Angelopoulos for the use of data from the THEMIS Mission. We also thank the NASA OMNIWeb for the solar wind and IMF data . We also thank the JHU/APL for making available the DMSP data. The authors also thank the International Space Science Institute in Beijing for supporting and hosting meetings of our International Team on "Multiple-instrument observations and simulations of the dynamical processes associated with polar cap patches/aurora and their associated scintillations, during which the discussions leading to this publication were initiated.

1. L. A. Frank *et al*., The theta aurora. *J. Geophys. Res.* **91**, 3177–3224 (1986).
2. L. Zhu, R. W. Schunk, J. J. Sojka, Polar cap arcs: A review. *J. Atmos. Sol. Terr. Phys.* **59**, 1087–1126 (1997).
3. A. Kullen, "Transpolar arcs: Summary and recent results" in *Auroral Phenomenology and Magnetospheric Processes: Earth And Other Planets*, A. Keiling, E. Donovan, F. Bagenal, T. Karlsson, Eds. (Geophysical Monograph, American Geophysical Union, Washington, DC, 2012), Vol. 197, pp. 69–80.
4. S. E. Milan, B. Hubert, A. Grocott, Formation and motion of a transpolar arc in response to dayside and nightside reconnection. *J. Geophys. Res.* **110**, A01212 (2005).
5. K. Hosokawa *et al*., Aurora in the polar cap: A review. *Space Sci. Rev.* **216**, 15 (2020).
6. C.-I. Meng, R. Lundin, Auroral morphology of the midday oval. *J. Geophys. Res.* **91**, 1572–1584 (1986).
7. R. C. Fear *et al*., Direct observation of closed magnetic flux trapped in the high-latitude magnetosphere. *Science* **346**, 1506–1510 (2014).
8. Z.-Y. Xing *et al*., Conjugate observations of the evolution of polar cap arcs in both hemispheres. *J. Geophys. Res. Space Phys.* **123**, 1794–1805 (2018).
9. Y. Zhang, L. J. Paxton, Q.-H. Zhang, Z. Xing, Polar cap arcs: Sun-aligned or cusp-aligned? *J. Atmos. Sol. Terr. Phys.* **146**, 123–128 (2016).
10. T. Yamamoto, M. Ozaki, A numerical model of the dayside aurora. *J. Geophys. Res.* **110**, A05215 (2005).
11. J. Reidy *et al*., Interhemispheric survey of polar cap aurora. *J. Geophys. Res. Space Phys.* **123**, 7283–7306 (2018).
12. J. A. Reidy *et al*., Multi-instrument observation of simultaneous polar cap auroras on open and closed magnetic field lines. *J. Geophys. Res. Space Phys.* **122**, 4367–4386 (2017).
13. J. W. Dungey, Interplanetary magnetic field and the auroral zones. *Phys. Rev. Lett.* **6**, 47 (1961).
14. Q.-H. Zhang *et al*., Direct observations of the evolution of polar cap ionization patches. *Science* **339**, 1597–1600 (2013).
15. Q. H. Zhang *et al*., Observations of the step-like accelerating processes of cold ions in the reconnection layer at the dayside magnetopause. *Sci. Bull.* **63**, 31–37 (2018).
16. S.-W. Chang *et al*., A comparison of a model for the theta aurora with observations from Polar, Wind, and SuperDARN. *J. Geophys. Res.* **103**, 17367–17390 (1998).
17. P. T. Newell, C.-I. Meng, Creation of theta-auroras: The isolation of plasma sheet fragments in the polar cap. *Science* **270**, 1338–1341 (1995).
18. B. V. Rezhenov, A possible mechanism for theta aurora formation. *Ann. Geophys.* **13**, 698–703 (1995).
19. I. V. Golovchanskaya, A. Kullen, Y. P. Maltsev, H. Biernat, Ballooning instability at the plasma sheet-lobe interface and its implications for polar arc formation. *J. Geophys. Res.* **111**, A11216 (2006).
20. A. Kozlovsky *et al*., Dynamics and electric currents of morningside Sun-aligned auroral arcs. *J. Geophys. Res.* **112**, A06306 (2007).
21. K. Makita, C.-I. Meng, S.-I. Akasofu, Transpolar auroras, their particle precipitation, and IMF by component. *J. Geophys. Res.* **96**, 14085–14095 (1991).
22. A. Kullen, The connection between transpolar arcs and magnetotail rotation. *Geophys. Res. Lett.* **27**, 73–76 (2000).
23. C. Y. Huang, J. D. Craven, L. A. Frank, Simultaneous observations of a theta aurora and associated magnetotail plasmas. *J. Geophys. Res.* **94**, 10137–10143 (1989).
24. T. Tanaka, T. Obara, M. Kunitake, Formation of the theta aurora by a transient convection during northward interplanetary magnetic field. *J. Geophys. Res.* **109**, A09201 (2004).
25. T. Tanaka *et al*., Formation of the Sun-aligned arc region and the void (polar slot) under the null-separator structure. *J. Geophys. Res.* **122**, 4102–4116 (2017).

26. H. Hasegawa *et al*., Transport of solar wind into Earth's magnetosphere through rolled-up Kelvin-Helmholtz vortices. *Nature* **430**, 755–758 (2004).
27. C. Wang *et al*., Magnetohydrodynamics (MHD) numerical simulations on the interaction of the solar wind with the magnetosphere: A review. *Sci. China Earth Sci.* **56**, 1141–1157 (2013).
28. X. Guo, C. Wang, Y. Hu, Global MHD simulation of the Kelvin-Helmholtz instability at the magnetopause for northward interplanetary magnetic field. *J. Geophys. Res.* **115**, A10218 (2010).
29. W. Li, C. Wang, B. Tang, X. Guo, D. Lin, Global features of Kelvin-Helmholtz waves at the magnetopause for northward interplanetary magnetic field. *J. Geophys. Res. Space Phys.* **118**, 5118–5126 (2013).
30. Q.-H. Zhang, H.-G. Yang, Z.-Y. Xing, Ground-based aurora data at Chinese Zhongshan Station for manuscript "Multiple transpolar auroral arcs reveal new insight about coupling processes in the Earth's magnetotail." Zenodo. http://doi.org/10.5281/zenodo.3778095. Deposited 30 April 2020.
31. R. Maggiolo *et al*., Polar cap ion beams during periods of northward IMF: Cluster statistical results. *Ann. Geophys.* **29**, 771–787 (2011).
32. R. Maggiolo *et al*., Polar cap arcs from the magnetosphere to the ionosphere: Kinetic modelling and observations by cluster and TIMED. *Ann. Geophys.* **30**, 283–302 (2012).
33. Y. Q. Hu, X. C. Guo, C. Wang, On the ionospheric and reconnection potentials of the Earth: Results from global MHD simulations. *J. Geophys. Res.* **112**, A07215 (2007).
34. B. B. Tang, C. Wang, Large scale current systems developed from substorm onset: Global MHD results. *Sci. China Technol. Sci.* **61**, 389–396 (2018).
35. Q.-H. Zhang, C. Wang, B.-B. Tang, Data of 3D MHD Simulation for manuscript "Multiple transpolar auroral arcs reveal insight about coupling processes in the Earth's magnetotail." Zenodo. http://doi.org/10.5281/zenodo.3777265. Deposited 30 April 2020.
36. S. Knight, Parallel electric felds. *Planet. Space Sci.* **21**, 741–750 (1973).
37. L. R. Lyons, "The field-aligned current versus electric potential relation and auroral electrodynamics" in *Physics of Auroral Arc Formation*, J. R. Kan, S.-I. Akasofu, Eds. (Geophysical Monograph, American Geophysical Union, Washington, DC, 1981), Vol. 25, p. 252.
38. V. Angelopoulos, *The THEMIS Mission* **141**, 5–34 (2008).
39. J. De Keyser, M. Echim, Electric potential differences across auroral generator interfaces. *Ann. Geophys.* **31**, 251–261 (2013).
40. J. De Keyser, M. Echim, M. Roth, Cross-field flow and electric potential in a plasma slab. *Ann. Geophys.* **31**, 1297–1314 (2013).
41. S. Wing, J. R. Johnson, Theory and observations of upward field-aligned currents at the magnetopause boundary layer. *Geophys. Res. Lett.* **42**, 9149–9155 (2015).
42. P. Colella, P. R. Woodward, The piecewise parabolic method (PPM) for gas-dynamical simulations. *J. Comput. Phys.* **54**, 174–201 (1984).